Geomechanics and Engineering, *Vol. 42, No. 6 (2025) 425-439*
https://doi.org/10.12989/gae.2025.42.6.425

Improved Timoshenko beam theory for mechanical and thermal flexural behavior of porous cross-ply laminated beams

Muayad A. Rajeh[1], Mohammed A. Al-Osta[1,2], Fouad Bourada[3], Abdeldjebbar Tounsi*[3,4], Abdelouahed Tounsi[1,2,3], Salah U. Al-Dulaijan[1,2] and Murat Yaylacı[5,6]

[1]*Department of Civil and Environmental Engineering, King Fahd University of Petroleum & Minerals, 31261 Dhahran, Eastern Province, Saudi Arabia*
[2]*Interdisciplinary Research Center for Construction and Building Materials, KFUPM, 31261 Dhahran, Saudi Arabia*
[3]*Material and Hydrology Laboratory, University of Sidi Bel Abbes, Faculty of Technology, Civil Engineering Department, Algeria*
[4]*Mechanical Engineering Department, Faculty of Science and Technology, University of Rélizane, Algeria*
[5]*Department of Civil Engineering, Recep Tayyip Erdogan University, 53100, Rize, Turkey*
[6]*Faculty of Turgut Kıran Maritime, Recep Tayyip Erdogan University, 53900, Rize, Turkey*

(*Received February 20, 2025, Revised August 30, 2025, Accepted September 1, 2025*)

Abstract. This article studies the flexural response of porous cross-ply laminated beams under sinusoidal mechanical and thermal loads. The sinusoidal thermal load is linearly varying in the transverse direction. For the first time, this work takes into consideration three porosity distribution models. Moreover, the analysis is performed via an improved Timoshenko beam theory that eliminates the need for a shear correction factor and introduces a parabolic distribution for the transverse shear strain. The beams are simply supported. The virtual work principle is utilized to derive the governing equations. The governing equations are then solved analytically via Navier's rule for the simple support condition. The present work's validity is checked by comparison with the results of Bernoulli Euler's classical, Timoshenko's first-order, Sayyad-Ghugal's trigonometric, Reddy's higher-order, and exact elasticity beam theories. The proposed theory is found to provide the closest results to those of the elasticity theory in comparison with the other theories. Parametric studies are conducted to measure the influence of porosity parameters on the response. Porosity distribution model 1 seems to have the greatest effect on the displacement results for both the thermal and mechanical load cases, followed by porosity model 2. In the mechanical load case, the lateral and axial displacements increase as the porosity volume fraction increases. However, the displacements for the thermal load case decrease as the porosity volume fraction increases.

Keywords: cross-ply laminated beam; distribution models; flexural analysis; improved Timoshenko beam theory; sinusoidal mechanical and thermal loads; thermal load; porosity; transverse linearly varying

1. Introduction

Laminated composite structures are increasingly used for their enhanced properties, weight reduction, and ability to be tailored for a given application. Given their excellent resistance (thermal and mechanical), composites have attracted a lot of attention and are used and applied in several fields, namely marine, automotive, aerospace and civil engineering. Entrapped air bubbles could accumulate during their production, affecting the laminates' mechanical behavior under load. Therefore, it's crucial to consider the porosities effect during analysis.

Numerous theories have been used for the analysis of laminated beams. The classical laminated beam theory (CBT), an extension of the Bernoulli-Euler beam theory, ignores the effect of transverse shear deformation (Tanigawa *et al.* 1989). However, transverse shear deformation has profound effects in laminated beams, rendering the analysis via CBT unfavorable (Sayyad and Ghugal 2011). Timoshenko's beam theory (TBT), also known as first-order shear deformation theory, considers a constant transverse shear stress across a beam's height. Although TBT provides better results than CBT, it requires a shear correction factor and doesn't satisfy the beam's top and bottom boundary conditions. For example, Chen et al. (2024) studied the dynamic response of the elastically supported bidirectional FG sandwich beam based on the Chebyshev collocation method, hamilton principle and first-order shear deformation theory. Subsequently, multiple higher-order shear deformation theories (HSDTs) were proposed to solve the deficiencies in CBT and TBT (Touratier 1991, Soldatos 1992, Khdeir and Reddy 1997, Matsunaga 2000, Kapuria *et al.* 2003, Karama *et al.* 2003, Reddy 2004, Aydogdu 2009, Akavci 2010, Emam 2011, Grover *et al.* 2013, Sahoo and Singh 2013, Kumar et al. 2015, Mehar and Panda 2018, Arani *et al*. 2019, Vinyas et *al.* 2020, Madenci and Özütok 2021, Frih *et al.* 2023, Turan 2024, Osman *et al*. 2024, Ozbey *et al.* 2024, Rajendran *et al.* 2024, Hadji *et al.* 2024).There are also other theories based 3D elasticity theory as used in the work of Bina et al. (2024) in which they examined the free vibration of FG laminated nanocomposite sandwich shells with wavy CNT-reinforced face sheets.

Several research studies were conducted on laminated beam analyses under thermal and mechanical loadings.

*Corresponding author, Professor
E-mail: abdeldjebbar.tounsi@univ-relizane.dz

ISSN: 2005-307X (Print), 2092-6219 (Online)

Khedeir and Reddy (1997) conducted a bending analysis of cross-ply laminated beams via CBT, TBT, and HSDTs. Kapuria *et al.* (2003) introduced a higher-order zigzag theory for simply supported laminated beam bending analysis under a thermal loading field. Beam's boundary conditions were satisfied, and a shear correction factor was not used. The virtual work principle was utilized to derive governing equations. Navier's method was used to obtain the analytical solution. Karama *et al.* (2003) proposed a novel multilayered model with transverse shear stress continuity for both static and dynamic response of laminated beams. The principle of virtual work was used to derive governing equations and boundary conditions. The results were compared with finite element software. Vidal and Polit (2006) performed a mechanical bending analysis of simply supported laminated beams under sinusoidal mechanical load via a refined finite element method with three nods. No shear correction factor was used, as the beam's top and bottom boundary conditions were satisfied. In another study, Vidal and Polit (2009) used a layer-refined sine-distribution-based finite element approach that includes a transverse normal strain effect for laminated beams' mechanical and thermo-mechanical static response. Introducing a cosine function in the transverse shear strain calculation eliminated the need for a shear correction factor. A study by Sayyad and Ghugal (2011) examined the influence of including a transverse normal deformation on the flexural analysis of simply supported laminated beams subjected to sinusoidal and uniformly distributed mechanical loads. The analysis was conducted using a trigonometric shear deformation theory (TrSDT) that doesn't require a shear correction factor. Both boundary conditions and governing equations were found via the virtual work principle. Murugesan and Rajamohan (2015) studied laminated beams combined with thermo-mechanical interlaminar stresses using finite element commercial software. Different boundary conditions and lamination sequences were considered. Mantari and Canales (2016) analyzed laminated beams under sinusoidal, uniformly distributed, linearly varying, and concentrated mechanical loads using a unified high-order shear deformation theory with the stretching effect. Kulkarni and Ghugal (2018) analyzed the thermo-mechanical flexural response of single, antisymmetric, and symmetric laminated beams via sinusoidal shear deformation theory. The beams are all simply supported. Ghalami-Choobar *et al.* (2018) used the unified zig-zag theory to perform static analysis of laminated composite beams under thermal and mechanical. Fang *et al.* (2019) studied the effects of porosity parameters on beam flexural analysis and free vibration via a quasi-3D method. The effects of normal deformation, shear deformation, and thickness stretching were considered. Srinivasan and Singh (2019) developed an exact unified state space theory for the flexural analysis of cross-ply laminated beams under mechanical load with various boundary conditions.

Since entrapped air voids are common during the fabrication of advanced composites, several studies were conducted to include their effect on composite structures' analysis results (Zhang *et al*. 2023, Xu and She 2023, Forou tan and Dai 2024, He and She 2024, Cui *et al*. 2024, Plevris *et al*. 2024, Pham *et al*. 2024, Ebrahimi *et al*. 2024, Shen *et al.* 2024, Li and She 2024, She *et al*. 2024). Yüksel and Akbaş (2019) examined the buckling behavior of laminated composite plates having porosity. The conventional first-order shear theory was used for the analysis. Navier's method was used to provide a simple support analytical solution. The effects of porosity volume, models, and lamination sequence on the response were studied. Kumar and Kumar (2022) examined the effect of evenly distributed porosity on laminated plates' flexural response via a third-order shear theory. Chen *et al.* (2015) investigated the buckling and bending of porous functionally graded (FG) beams under uniformly distributed and concentrated loads using TBT. Hamilton's principle was employed to derive the governing equations. Transverse bending was obtained through the Ritz rule. Various boundary conditions were considered. Recently, the nonlinear forced vibration of FG with initial geometrical defects in hygro-thermal ambiences is investigated by He and She (2024) based on the Euler Bernoulli beam theory, Hamiltonian principle and geometrical non-linearity. Cui *et al.* (2024) examined the effect of porosity on the response of the nanoparticles reinforced nanocomposite under sinusoidal transverse dynamic force based on the Aydogdu shear deformation theory (ASDT) and Ritz method. Pham *et al.* (2024) analyzed the vibrational response of the variable thickness imperfect FG porous microplates under the effects of hygro-thermal environment via refined higher-order shear deformation plate theory (RPT) in construction with the modified couple stress theory. Nonlinear vibrational characteristic of porous cylindrical shells covered by CNTs-reinforced nanocomposite layers is investigated by Liu *et al*. (2024) based on the FSDT beam theory, Von-Karman formulation and Galerkin's approach.

The aforementioned literature survey detects knowledge gaps in consideration of different porosity distribution models for the analysis of porous laminated composite beams' static and dynamic responses, with little consideration of the porosity effect on the flexural behavior of laminated composite beams. This article aims to examine the sinusoidal mechanical and thermal loads flexural response of porous cross-ply laminated beams via an improved TBT. The thermal load will vary linearly in thickness direction. The proposed theory discards the use of a shear correction factor. The present method's findings will be compared with CBT, conventional TBT, TrSDT, HSDT, and exact elasticity theory. The effects of porosity volume fraction variation and three porosity distribution models on the flexural response will be checked.

2. Theoretical formulation

Consider a simply supported laminated beam of rectangular shape with n number of orthotropic laminae, length a, width b (where $b << a$), and total thickness h as shown in Fig. 1. The x-y plane goes through the middle of the beam. The beam is subjected to a thermal load $T(x, z)$ and mechanical load q.

The porosity is distributed through each lamina. Three distribution models are considered, as Fig. 2 depicts.

In model 1, the micro-voids are evenly distributed along the lamina's thickness; in model 2, these voids are concentrated in the lamina's top and bottom surfaces. In model 3, the voids are more condensed in the middle

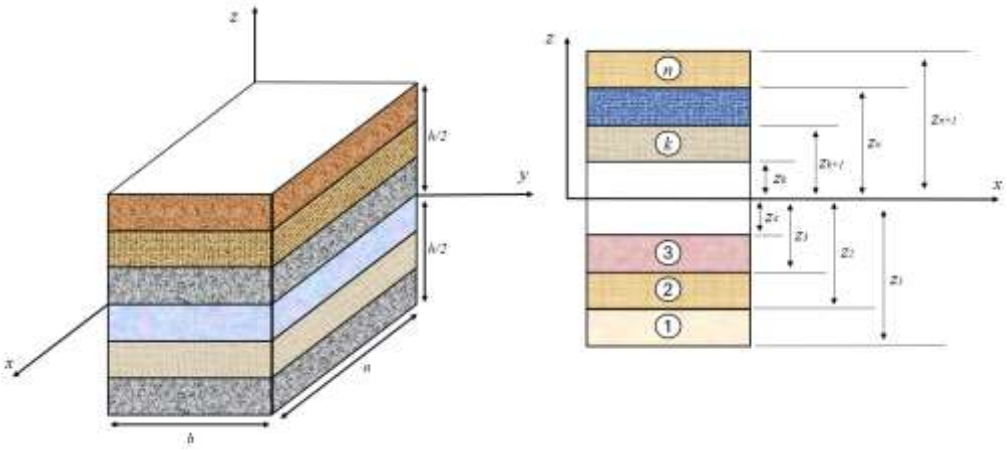

Fig. 1 Geometry and coordinate system of the beam

Fig. 2 Illustration of porosity distribution models

Table 1 Material effective properties expression under porosity influence

Porosity distribution models	The material property (*P*)
Model 1	$P(\xi) = P(1-\xi)$
Model 2	$P(\xi) = P\left(1-\xi\frac{2\lvert z\rvert}{h}\right)$
Model 3	$P(\xi) = P\left(1-\frac{\xi}{2}\left(1-\frac{2\lvert z\rvert}{h}\right)\right)$

where ξ represents the porosity volume fraction. $\xi = 0$ means a porous-free beam

portion of the lamina.

Porosities will reduce the effective properties (P) of a lamina, such as Young's moduli (E), shear moduli (G), Poisson's ratios (v), and the coefficients of thermal expansion (α). The mathematical expressions of the porosity models are presented in Table 1.

2.1 Kinematics

The beam's behavior will be described using an improved Timoshenko's beam theory (I-TBT). In I-TBT, the transverse deflection w is partitioned into a bending component w_b and a shear component w_s.

$$u(x,z) = u_0(x) - z\,\frac{\partial w_b(x)}{\partial x}$$
$$w(x,z) = w_b(x) + w_s(x) \tag{1}$$

The unknowns are $u_0, w_b, and\ w_s$. $u\ and\ w$ are the displacement of a point in the x and z directions, respectively. And u_0 is the middle plane deformations along x.

The normal strain according to assumptions is

$$\{\epsilon_x\} = \{\epsilon_x^0\} + z\{\kappa_x^b\} \tag{2a}$$

where

$$\{\epsilon_x^0\} = \left\{\frac{\partial u_0}{\partial x}\right\}; \quad \{\kappa_x^b\} = \left\{-\frac{\partial^2 w_b}{\partial x^2}\right\} \tag{2b}$$

The transverse shear strain is

$$\{\gamma_{xz}^s\} = \left\{\frac{\partial w_s}{\partial x}\right\} \tag{3a}$$

However, a shear distribution function $g(z)$ is introduced to improve TBT's transverse shear distribution along the thickness and eliminate the need for a shear correction factor. So, the shear strain becomes

$$\{\gamma_{xz}\} = g(z)\{\gamma_{xz}^s\} \tag{3b}$$

Where

$$g(z) = 1.35 - 5.4\,\frac{z^2}{h^2} \tag{3c}$$

2.2 Constitutive equations

The local stress-strain relationships for a single lamina in plane stress condition, including temperature and porosity effects, are

$$\begin{Bmatrix}\sigma_x\\ \sigma_y\\ \tau_{xy}\end{Bmatrix} = \begin{bmatrix}Q_{11}(\xi) & Q_{12}(\xi) & 0\\ Q_{12}(\xi) & Q_{22}(\xi) & 0\\ 0 & 0 & Q_{66}(\xi)\end{bmatrix} \begin{Bmatrix}\epsilon_x - \alpha_x(\xi)\,T\\ \epsilon_y - \alpha_y(\xi)\,T\\ \gamma_{xy} - \alpha_{xy}(\xi)\,T\end{Bmatrix} \quad (4a)$$

$$\begin{Bmatrix}\tau_{yz}\\ \tau_{xz}\end{Bmatrix} = \begin{bmatrix}Q_{44}(\xi) & 0\\ 0 & Q_{55}(\xi)\end{bmatrix} \begin{Bmatrix}\gamma_{yz}\\ \gamma_{xz}\end{Bmatrix} \quad (4b)$$

$Q_{ij}(\xi)$ are the reduced stiffnesses that are linked to the lamina engineering constants as Eq. (5) states.

$$Q_{11}(\xi) = \frac{E_1(\xi)}{1 - v_{12}(\xi)\,v_{21}(\xi)},\ Q_{12}(\xi) = \frac{v_{12}\,E_2(\xi)}{1 - v_{12}(\xi)\,v_{21}(\xi)},\quad Q_{22}(\xi) = \frac{E_2(\xi)}{1 - v_{12}(\xi)\,v_{21}(\xi)} \quad (5a)$$

$$Q_{44}(\xi) = G_{23}(\xi), Q_{55}(\xi) = G_{13}(\xi), Q_{66}(\xi) = G_{12}(\xi \quad (5b)$$

The temperature field variation T(x, z) is assumed to be linearly varying along the beam thickness according to the function ($\frac{2\,z}{h}$), and is defined as

$$T(x,z) = \frac{2\,z}{h}\,T_1(x) \quad (6)$$

The constitutive relation of the beam's kth lamina transformed from the local to the global (*x, y, z*) coordinate system is below.

$$\begin{Bmatrix}\sigma_x\\ \tau_{xz}\end{Bmatrix}_k = \begin{bmatrix}\bar{Q}_{11}(\xi) & 0\\ 0 & \bar{Q}_{55}(\xi)\end{bmatrix}_k \begin{Bmatrix}\epsilon_x - \alpha_x(\xi)\,T\\ \gamma_{xz}\end{Bmatrix}_k \quad (7)$$

$\bar{Q}_{ij}(\xi)$ are the transformed reduced stiffnesses, calculated as

$$\bar{Q}_{11}(\xi) = Q_{11}(\xi)cos^4(\theta) + Q_{22}(\xi)sin^4(\theta) + 2\big(Q_{12}(\xi) + 2Q_{66}(\xi)\big)cos^2(\theta)sin^2(\theta) \quad (8a)$$

$$\bar{Q}_{55}(\xi) = Q_{55}(\xi)\,cos^2(\theta) + Q_{44}(\xi)\,sin^2(\theta) \quad (8b)$$

$\alpha_x^{(k)}(\xi)$ is the transformed coefficient of thermal expansion, defined as

$$\alpha_x^{(k)}(\xi) = \alpha_x(\xi)\,cos^2(\theta) + \alpha_y(\xi)\,sin^2(\theta) \quad (9)$$

Where θ is the angle of transformation, positive measured counterclockwise going from the global to the local axes.

2.3 Governing equations

By integrating (7) through the thickness, stress resultants are found as follows

$$\begin{Bmatrix}N_x\\ M_x^b\end{Bmatrix} = \begin{bmatrix}A_{11} & B_{11}\\ B_{11} & D_{11}\end{bmatrix}\begin{Bmatrix}\epsilon_x^0\\ \kappa_x^b\end{Bmatrix} - \begin{Bmatrix}N_x^T\\ M_x^{bT}\end{Bmatrix} \quad (10a)$$

$$\{S_{xz}^s\} = [A_{55}^s]\,\{\gamma_{xz}^s\} \quad (10b)$$

where these stiffnesses are defined as (Ekmon *et al.* 2024)

$$(A_{11}, B_{11}, D_{11}) = \sum_{k=1}^{n}\int_{z_k}^{z_{k+1}} \bar{Q}_{11}^{(k)}(\xi)\,(1, z, z^2)dz \quad (11a)$$

$$(A_{55}^s) = \sum_{k=1}^{n}\int_{z_k}^{z_{k+1}} \bar{Q}_{55}^{(k)}(\xi)\,g^2(z)dz \quad (11b)$$

The laminated beam's governing equations are derived using the virtual work principle (Basem et al. 2024), as shown below.

$$\int_{-\frac{h}{2}}^{\frac{h}{2}}\int_0^a (\sigma_x\,\delta\epsilon_x + \tau_{xz}\,\delta\gamma_{xz})dx\,dz - \int_0^a q\,\delta w\ dx = 0 \quad (12)$$

Substituting (2-7) into (12), and performing the integration along *z*

$$\int_0^a \left(N_x\frac{\partial\,\delta u_0}{\partial x} - M_x^b\frac{\partial^2\,\delta w_b}{\partial x^2} + S_{xz}^s\frac{\partial\,\delta w_s}{\partial x} - q\,\delta w\right)dx = 0 \quad (13)$$

Performing integration by parts and collecting the unknowns $\delta u_0, \delta w_b, \delta w_s$ coefficients, the governing equations become

$$\delta u_0 : \frac{\partial\,N_x}{\partial x} = 0$$

$$\delta w_b : \frac{\partial^2\,M_x^b}{\partial x^2} + q = 0 \quad (14)$$

$$\delta w_s : \frac{\partial\,S_{xz}^s}{\partial x} + q = 0$$

Substituting (10) into (14), the governing equations in terms of displacements are

$$\delta u_0 :\ A_{11}\frac{\partial^2 u_0}{\partial x^2} - B_{11}\frac{\partial^3 w_b}{\partial x^3} - \frac{\partial\,N_x^T}{\partial x} = 0 \quad (15a)$$

$$\delta w_b :\ B_{11}\frac{\partial^3 u_0}{\partial x^3} - D_{11}\frac{\partial^4 w_b}{\partial x^4} - \frac{\partial^2\,M_x^{bT}}{\partial x^2} + q = 0 \quad (15b)$$

$$\delta w_s :\ A_{55}^s\frac{\partial^2\,w_s}{\partial x^2} + q = 0 \quad (15c)$$

3. Analytical solution

Here, we concern with the close form solutions (Navier's method) of simply anti-symmetric cross-ply laminated beam. The boundary conditions for simply supported edges are

$$w_b = w_s = N_x = M_x^b = 0,\quad at\ x = 0, x = a \quad (16)$$

The deflection and resultants moments are equal zero at the limit edges because the supports will prevent vertical displacement so $w_b = w_s = 0$ and the rotation exist which gives a null moment.

The loads are written in Fourier series expansion as

$$\begin{Bmatrix}T_1(x)\\ q(x)\end{Bmatrix} = \sum_{m=1}^{\infty}\begin{Bmatrix}T_{1m}\\ q_m\end{Bmatrix}sin(\mu\,x) \quad (17a)$$

where T_{1_m}, $and\ q_m$ are stated as

$$\begin{Bmatrix} T_{1_m} \\ q_m \end{Bmatrix} = \frac{2}{a}\int_0^a \begin{Bmatrix} T_1(x) \\ q(x) \end{Bmatrix} sin(\mu\, x)\, dx \tag{17b}$$

and $\mu = \frac{m\,\pi}{a}$.

Considering a single sinusoidal thermal and mechanical loading, then $T_{1_m} = T_0$ and $q_m = q_0$ when (17b) is integrated for $m = 1$. T_0, and q_0 are the loads' maximum intensity.

The unknown's $u_0, w_b, and\ w_s$ solution form is expressed as

$$\begin{Bmatrix} u_0 \\ w_b \\ w_s \end{Bmatrix} = \sum_{m=1}^{\infty} \begin{Bmatrix} U_m\, cos(\mu\, x) \\ W_{b_m}\, sin(\mu\, x) \\ W_{s_m}\, sin(\mu\, x) \end{Bmatrix} \tag{18}$$

where the parameters U_m, W_{b_m}, W_{s_m} are arbitrary. Substituting (17-18) into (15), the following algebraic operator equation is formed

$$\begin{bmatrix} K_{11} & K_{12} & K_{13} \\ K_{12} & K_{22} & K_{23} \\ K_{13} & K_{23} & K_{33} \end{bmatrix} \begin{Bmatrix} U_m \\ W_{b_m} \\ W_{s_m} \end{Bmatrix} = \begin{Bmatrix} F_1 \\ F_2 \\ F_3 \end{Bmatrix} \tag{19}$$

where

$$\begin{aligned} K_{11} &= -A_{11}\,\mu^2 \\ K_{12} &= B_{11}\,\mu^3 \\ K_{13} &= 0 \\ K_{22} &= -D_{11}\,\mu^4 \\ K_{23} &= 0 \\ K_{33} &= -A^s_{55}\,\mu^2 \end{aligned} \tag{20}$$

and

$$\begin{aligned} F_1 &= 2\,P_{11}\,T_{1_m}\,\mu \\ F_2 &= -2\,F_{11}\,T_{1_m}\,\mu^2 - q_m \\ F_3 &= -q_m \end{aligned} \tag{21}$$

Where the laminate stiffness coefficients appear in the above the generalized force vector (Eq. (21)) are

$$(P_{11}) = \sum_{k=1}^{n} \int_{z_k}^{z_{k+1}} \alpha_x^{(k)}(\xi)\, \bar{Q}_{11}^{(k)}(\xi)\, \left(\frac{z}{h}\right) dz \tag{22a}$$

$$(F_{11}) = \sum_{k=1}^{n} \int_{z_k}^{z_{k+1}} \alpha_x^{(k)}(\xi)\, \bar{Q}_{11}^{(k)}(\xi)\, \left(\frac{z^2}{h}\right) dz \tag{22b}$$

4. Numerical results and discussion

This section is partitioned into two parts. The first part is concerned with the validation of the I-TBT model's accuracy and studies the porous laminated beam bending response under a transverse mechanical load. The second part examines the thermal bending response of the porous laminated beam. In both parts, the influences of porosity parameters' variation are investigated. Consider a porous simply supported anti-symmetric cross-ply laminated beam of the lamination scheme (0°/90°). The perfect porous-free lamina material properties are taken as (Bhaskar *et al.* 1996, Sayyad and Ghugal 2011)

$$\begin{aligned} &\frac{E_1}{E_2} = 25, \quad G_{12} = G_{13} = 0.5\,E_2, \quad G_{23} = 0.2\,E_2, \\ &v_{12} = 0.25, \quad \frac{\alpha_2}{\alpha_1} = 1125 \end{aligned} \tag{23}$$

4.1 Mechanical flexural behavior of porous laminated beams

For the (0°/90°) laminated beam, the mechanical load dimensionless displacements and stresses are stated in a (x, z) coordinate fashion as shown below.

$$\begin{aligned} \bar{u} = \frac{E_2\, b}{q_0\, h} u\left(0, \frac{z}{h}\right), \bar{w} = \frac{100 E_2}{q_0\, h\, s^4} w\left(\frac{a}{2}, \frac{z}{h}\right), \\ \bar{\sigma}_x = \frac{b}{q_0} \sigma_x\left(\frac{a}{2}, \frac{z}{h}\right), \\ \bar{\tau}_{xz} = \frac{b}{q_0} \tau_{xz}\left(0, \frac{z}{h}\right) \end{aligned} \tag{24}$$

where $s = \frac{a}{h}$.

The numerical results of the present theory (I-TBT) for the flexural response of a two-lamina anti-symmetric cross-ply laminated beam for both perfect and porous beams under transverse sinusoidal mechanical load are demonstrated in Table 2. The perfect beam's results are compared with Bernoulli Euler's CBT, Timoshenko's TBT, Sayyad-Ghugal's TrSDT, Reddy's HSDT, and exact elasticity theory (Sayyad and Ghugal 2011).

In the case of the porous-free beam, the present I-TBT theory predicted very close results with those of exact, HSDT, and TrSDT theories in the calculation of the transverse shear stress obtained through constitutive relations $\bar{\tau}_{xz}^{CR}(0)$. For the lateral deflection $\bar{w}(0)$ prediction, I-TBT is consistent with TBT, TrSDT, HSDT, and exact theory results. The maximum transverse shear stress was calculated using the 3-D equilibrium equations $\bar{\tau}_{xz}^{EE}(max)$, all theories predict similar results. The axial stress $\bar{\sigma}_x(-\frac{h}{2})$ and axial displacement $\bar{u}(-\frac{h}{2})$ are both underestimated by CBT, TBT, and I-TBT. Whereas TrSDT and HSDT overestimate them.

For the porous beam, Table 2 reveals that $\bar{u}(-\frac{h}{2})$ and $\bar{w}(0)$ are affected the most, in decreasing order, by porosity distribution models 1, 2, and then 3. As the porosity volume fraction increases, both $\bar{u}(-\frac{h}{2})$ and $\bar{w}(0)$ increase regardless of the distribution model. Furthermore, $\bar{\sigma}_x(-\frac{h}{2})$, $\bar{\tau}_{xz}^{CR}(0)$, and $\bar{\tau}_{xz}^{EE}(max)$ are affected the most by porosity model 2, followed by model 3, while model 1 doesn't seem to affect them. As ξ increases, the magnitude of $\bar{\sigma}_x(-\frac{h}{2})$ decreases in porosity model 2, however, it increases in model 3. On the contrary, as ξ increases both transverse shear stresses increase for porosity model 2 and decrease for model 3.

In Fig. 3, I-TBT is used to draw normalized results variation considering ξ values from 0.0 to 0.5 for porosity model 1. Similarly, the normalized results for porosity models 2 and 3 are shown in Figs. 4 and 5, respectively.

Table 2 Dimensionless displacements and stresses for two layers (0°/90°) anti-symmetric cross-ply laminated composit perfect and porous beams under transverse sinusoidal mechanical load ($T = 0$)

s	Model	Theory		$\bar{u}(-h/2)$	$\bar{w}(0)$	$\bar{\sigma}_x(-h/2)$	$\bar{\tau}_{xz}^{CR}(0)$	$\bar{\tau}_{xz}^{EE}(*)$
4	Exact	Elasticity [a]		1.5288	4.7080	-30.0190	2.7212	-
	CBT	Bernoulli-Euler [a]		1.4176	2.6188	-27.9049	-	2.9468
	TBT	Timoshenko [a]		1.4176	4.4281	-27.9049	1.8189	2.9468
	HSDT	Reddy [a]		1.7108	4.4511	-33.5921	2.4769	2.9768
	TrSDT	Sayyad and Ghugal (2011)		1.7183	4.3955	-33.8252	2.5185	2.9885
	I-TBT	Present	Perfect	1.4176	4.4803	-27.9049	2.5263	2.9503
		Present (Model-1)	$\xi = 0.1$	1.5759	4.9795	-27.9049	2.5263	2.9503
			$\xi = 0.2$	1.7736	5.6033	-27.9049	2.5263	2.9503
			$\xi = 0.3$	2.0278	6.4052	-27.9049	2.5263	2.9503
			$\xi = 0.4$	2.3665	7.4741	-27.9049	2.5263	2.9503
			$\xi = 0.5$	2.8406	8.9704	-27.9049	2.5263	2.9503
	I-TBT	Present (Model-2)	$\xi = 0.1$	1.5326	4.7105	-27.1380	2.6078	2.9713
			$\xi = 0.2$	1.6683	4.9722	-26.2473	2.6947	2.9964
			$\xi = 0.3$	1.8310	5.2736	-25.1970	2.7876	3.0253
			$\xi = 0.4$	2.0299	5.6264	-23.9352	2.8872	3.0604
			$\xi = 0.5$	2.2786	6.0485	-22.3839	2.9941	3.1022
	I-TBT	Present (Model-3)	$\xi = 0.1$	1.4361	4.6002	-28.2676	2.4854	2.9398
			$\xi = 0.2$	1.4551	4.7281	-28.6421	2.4415	2.9286
			$\xi = 0.3$	1.4747	4.8647	-29.0291	2.3942	2.9182
			$\xi = 0.4$	1.4951	5.0110	-29.4295	2.3432	2.9071
			$\xi = 0.5$	1.5162	5.1683	-29.8444	2.2879	2.8951
10	Exact	Elasticity [a]		22.4760	2.9611	-176.530	7.2678	-
	CBT	Bernoulli-Euler [a]		22.1505	2.6188	-174.4052	-	7.3670
	TBT	Timoshenko [a]		22.1505	2.9083	-174.4052	4.5473	7.3670
	HSDT	Reddy [a]		22.9424	2.9225	-180.1890	6.2973	7.3780
	TrSDT	Sayyad and Ghugal (2011)		22.9353	2.9113	-180.5434	6.4254	7.3845
	I-TBT	Present	Perfect	22.1505	2.9167	-174.4050	6.3157	7.3757
		Present (Model-1)	$\xi = 0.1$	24.6233	3.2421	-174.4050	6.3157	7.3757
			$\xi = 0.2$	27.7131	3.6488	-174.4050	6.3157	7.3757
			$\xi = 0.3$	31.6840	4.1714	-174.4050	6.3157	7.3757
			$\xi = 0.4$	36.9766	4.8681	-174.4050	6.3157	7.3757
			$\xi = 0.5$	44.3842	5.8432	-174.4050	6.3157	7.3757
	I-TBT	Present (Model-2)	$\xi = 0.1$	23.9466	3.0965	-169.6120	6.5194	7.4283
			$\xi = 0.2$	26.0669	3.3044	-164.0460	6.7367	7.4909
			$\xi = 0.3$	28.6094	3.5482	-157.4810	6.9690	7.5632
			$\xi = 0.4$	31.7165	3.8395	-149.5950	7.2179	7.6510
			$\xi = 0.5$	35.6028	4.1953	-139.8990	7.4852	7.7554
	I-TBT	Present (Model-3)	$\xi = 0.1$	22.4384	2.9810	-176.6720	6.2135	7.3494
			$\xi = 0.2$	22.7356	3.0491	-179.0130	6.1037	7.3214
			$\xi = 0.3$	23.0428	3.1213	-181.4320	5.9856	7.2955
			$\xi = 0.4$	23.3607	3.1982	-183.9340	5.8580	7.2678
			$\xi = 0.5$	23.6901	3.2802	-186.5280	5.7199	7.2378

[a] From Ref. (Sayyad and Ghugal 2011); * Designates the maximum $\bar{\tau}_{xz}^{EE}$ magnitude

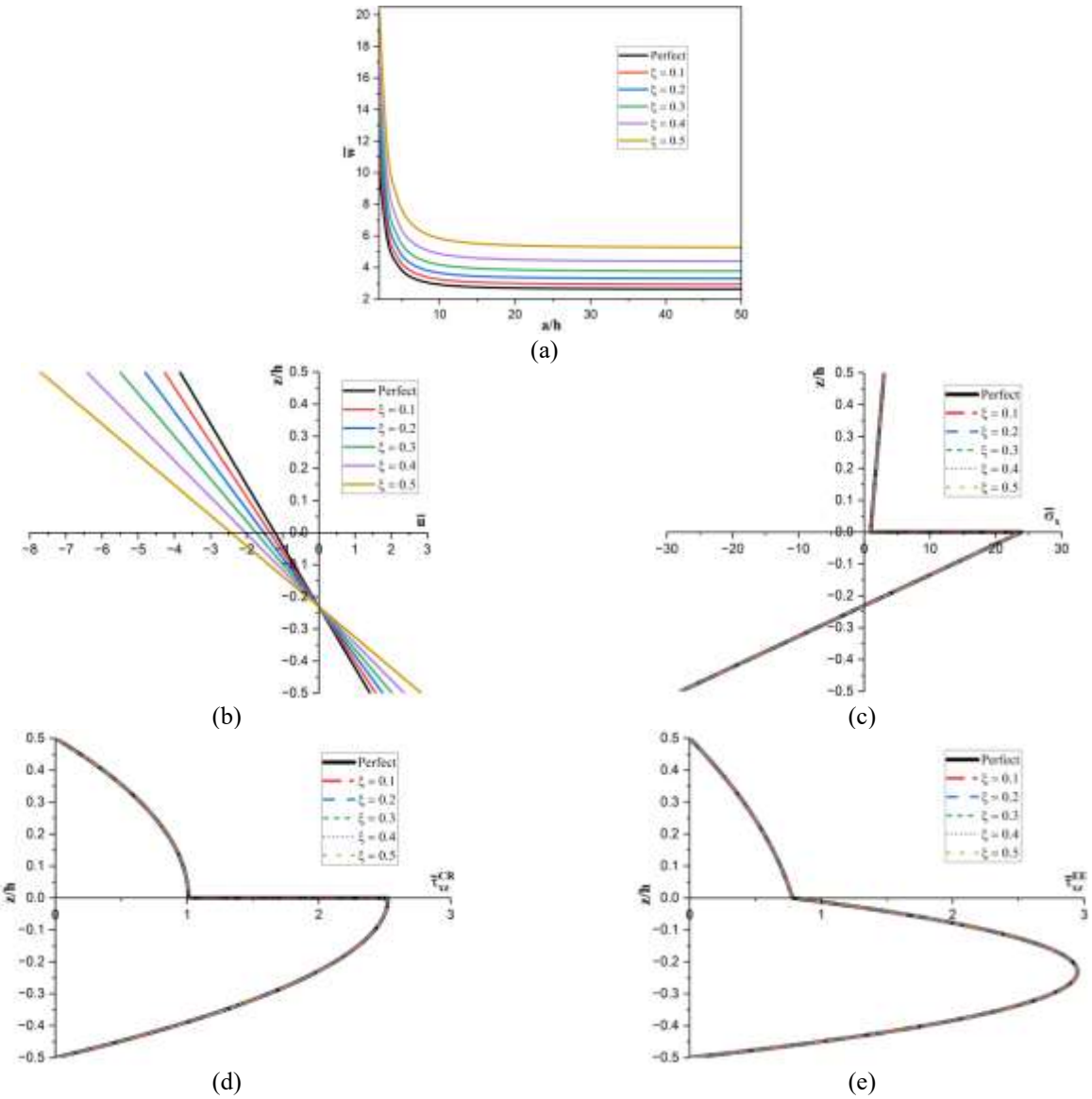

Fig. 3 Variation of dimensionless stresses and displacements for the (0°/90°) porous laminated beam under transverse sinusoidal mechanical load according to porosity distribution model 1 with $\frac{a}{h} = 4$: (a) lateral deflection $\overline{w}$ vs. *a/h*, (b) axial displacement $\bar{u}$ vs. *z/h*, (c) axial stress $\bar{\sigma}_x$ vs. *z/h*, (d) out-of-plane shear stress $\bar{\tau}_{xz}^{CR}$ vs. *z/h* and (e) out-of-plane shear stress $\bar{\tau}_{\mathrm{xz}}^{EE}$ vs. *z/h*

Figs. 3(a) and 3(b) show that at any z location, as ξ increases the values of $\overline{w}$, and $\bar{u}$ increase too. In Fig. (a), as the aspect ratio enlarges for the perfect beam, the I-TBT deflection reaches the CBT results. Figs. 3(c)-3(e) illustrations confirm that model 1 porosity doesn't effect on $\bar{\sigma}_x$, $\bar{\tau}_{xz}^{CR}$, and $\bar{\tau}_{xz}^{EE}$ under the mechanical induced response.

For porosity distribution model 2, Fig. 4(b) shows that at any z location, except from $z/h = (-1.5 \text{ to } -2.2)$, as the porosity volume fraction increases, the magnitude of $\bar{u}$ increase as well. Fig. 4(c) depicts that as the beam moves from $\xi = 0.0$ to 0.5 the maximum value for $\bar{\sigma}_x$ shifts from $z = -h/2$ to $z = 0$ in the (0°) lamina. Figs. 4(d) and 4(e) illustrate that as ξ increases, the transverse shear stresses' maximum value increases as well.

Figs. 5(a)-5(e) show that porosity model 3 does affect the beam's mechanically induced flexural response, but rather minimally. Nonetheless, generally as ξ increases $\overline{w}$, and $\bar{u}$ increase also. Fig. 5(d) demonstrates that the porosity according to model 3 primarily affects the $\bar{\tau}_{xz}^{CR}$ at the laminae interface, at which as porosity volume fraction increases, the transverse shear stresses decrease. Fig. 6 graphs compare the effects of porosity models at ξ = 0.2 on the (0°/90°) laminated beam's dimensionless stresses and displacements. In Figs. 6(a) and 6(b), porosity model 1 seems to have a greater effect on the transverse and axial displacements, followed by model 2. However, when it comes to the stresses, model 1 doesn't affect them, with the highest impact due to porosity by model 2, then model 3, as Figs. 6(c) and 6(e) shows. For the axial stress, the porosity model 2 tends to have the maximum magnitude at $z = 0$, while for model 3, the maximum is at $z = -h/2$, as portrayed by Fig. 6(c). Fig. 6(d) shows that at $(\frac{z}{h} = 0)$ for a

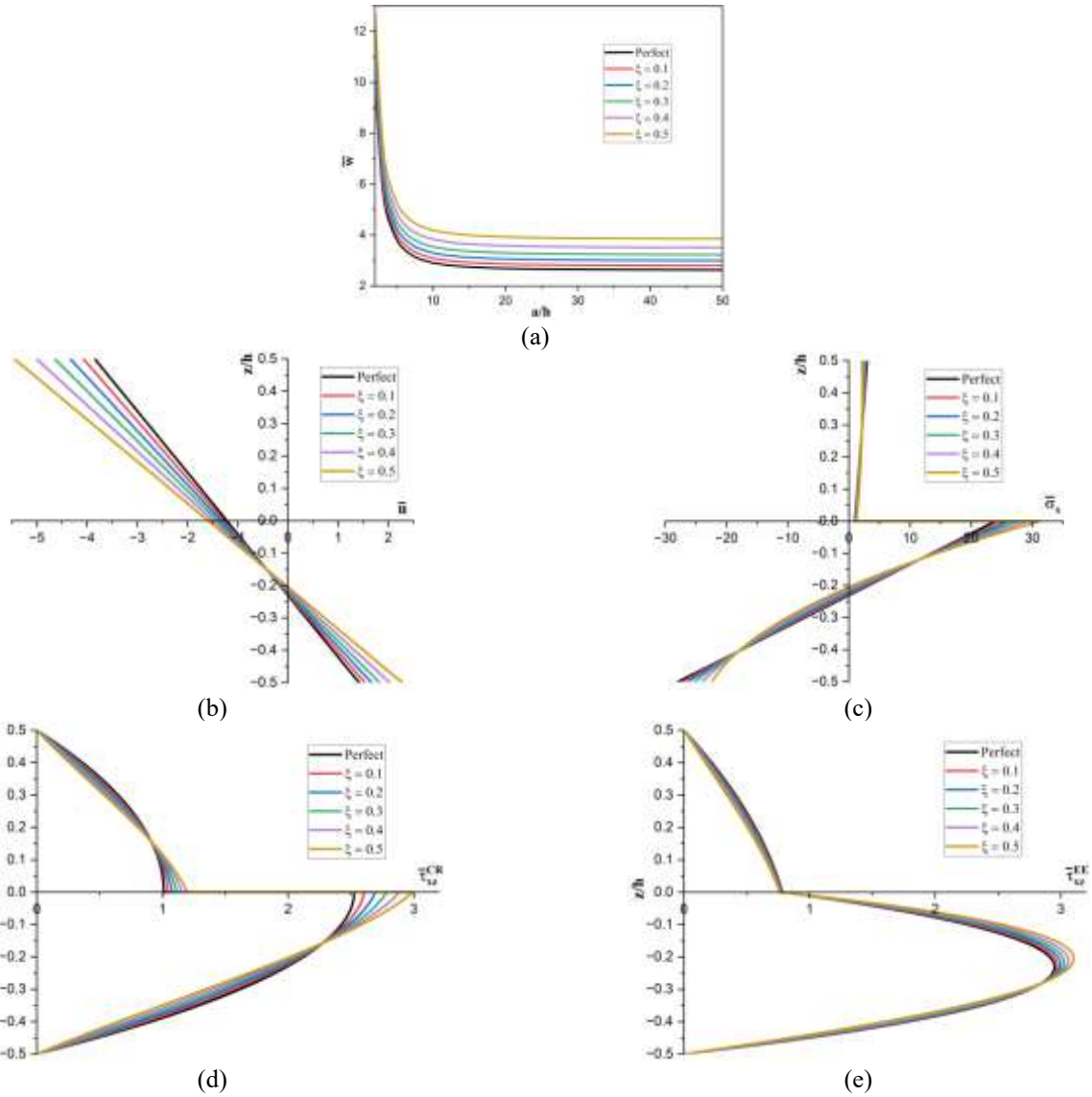

Fig. 4 Variation of dimensionless stresses and displacements for the (0°/90°) porous laminated beam under transverse sinusoidal mechanical load according to porosity distribution model 2 with $\frac{a}{h} = 4$: (a) lateral deflection $\bar{w}$ vs. *a/h*, (b) axial displacement $\bar{u}$ vs. *z/h*, (c) axial stress $\bar{\sigma}_x$ vs. *z/h*, (d) out-of-plane shear stress $\bar{\tau}_{xz}^{CR}$ vs. *z/h and* (e) out-of-plane shear stress $\bar{\tau}_{xz}^{EE}$ vs. *z/h*

constant ξ, $\bar{\tau}_{xz}^{CR}$ increases by porosity model 2 and decreases by model 3.

4.2 Thermal Flexural Behavior of Porous Laminated Beams

For the (0°/90°) laminated beam, the sinusoidal linearly varying thermal load dimensionless displacements and stresses are stated in a (x, z) coordinate as follows

$$\bar{u} = \frac{u}{\alpha_1 T_0 a}\left(0, \frac{z}{h}\right), \bar{w} = \frac{h w}{\alpha_1 T_0 a^2}\left(\frac{a}{2}, 0\right),$$
$$\bar{\sigma}_x = \frac{\sigma_x}{E_2 \alpha_1 T_0}\left(\frac{a}{2}, \frac{z}{h}\right), \bar{\tau}_{xz} = \frac{\tau_{xz}}{E_2 \alpha_1 T_0}\left(0, \frac{z}{h}\right) \quad (25)$$

τ_{xz} is calculated by the equilibrium equations.

Table 3 provides I-TBT's numerical solution for the flexural behavior of a two-layer cross-ply laminated beam with $\frac{a}{h} = 4$, in view of all porosity models with $\xi = (0.1 - 0.5)$, subjected to the linear sinusoidal thermal load expressed in (6) and (17) with $q = 0$. The porosity distribution model 1 has the greatest effect on the results, followed by model 2.

As ξ increases in porosity model 1 and model 2, the magnitude of $\bar{u}(h/2)$, $\bar{w}$, $\bar{\sigma}_x(-h/2)$, and $\bar{\tau}_{xz}^{EE}$ (0) decrease significantly. Porosity model 3, on the other hand, has marginal effects on $\bar{u}(h/2)$, $\bar{w}$, and $\bar{\sigma}_x(-h/2)$. But, in model 3 as the porosity volume fraction increases $\bar{w}$, $\bar{\sigma}_x(-h/2)$, and $\bar{\tau}_{xz}^{EE}$ (0) decrease.

Fig. 7 demonstrates the normalized results for porosity model 1. Similarly, Figs. 8 and 9 depict the normalized

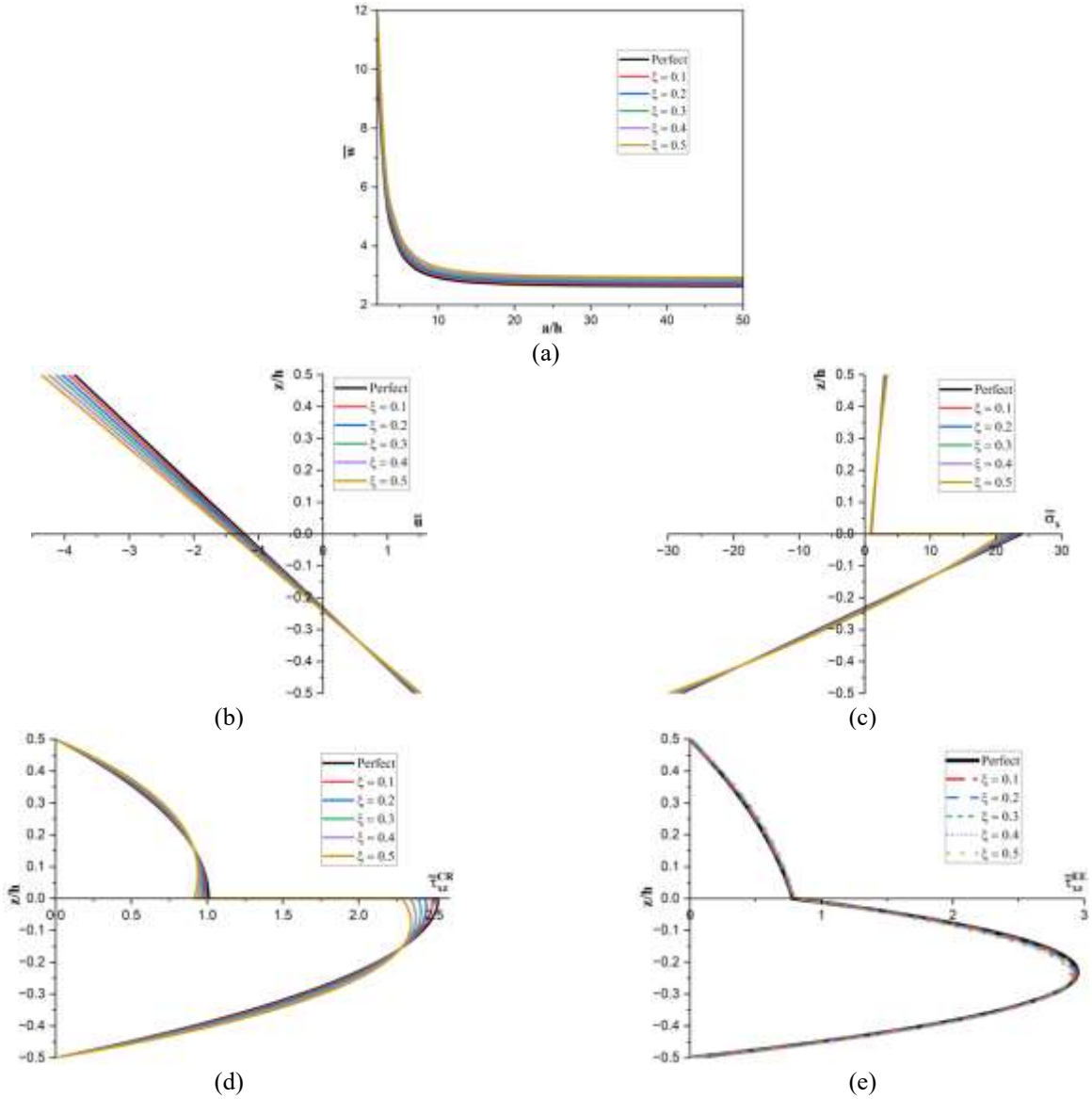

Fig. 5 Variation of dimensionless stresses and displacements for the (0°/90°) porous laminated beam under transverse sinusoidal mechanical load according to porosity distribution model 3 with $\frac{a}{h} = 4$: (a) lateral deflection $\bar{w}$ vs. *a/h*, (b) axial displacement $\bar{u}$ vs. *z/h*, (c) axial stress $\bar{\sigma}_x$ vs. *z/h*, (d) out-of-plane shear stress $\bar{\tau}_{xz}^{CR}$ vs. *z/h* and (e) out-of-plane shear stress $\bar{\tau}_{\mathrm{xz}}^{EE}$ vs. *z/h*

solution for models 2 and 3, respectively. As ξ increases for porosity model 1, the magnitudes of $\bar{u}$, $\bar{\sigma}_x$, and $\bar{\tau}_{xz}^{EE}$ considerably decrease at any given z location, as manifested in Figs. 7(a)-7(c). This could be attributed to the thermal insulation capabilities of porosity air pockets. Although Fig. 7(b) displays that $\bar{\sigma}_x$ discontinuity at the laminae border decreases as the volume fraction of porosity model 1 increases, the maximum axial stress's magnitude is at the (0°) lamina side of the border ($z = 0$). $\bar{\tau}_{xz}^{EE}$ on the other hand, has its maximum value at ($\frac{z}{h} = -0.28$) for all ξ as Fig. 7(c) reveals.

For porosity model 2 also, as ξ increases the magnitudes of $\bar{u}$, $\bar{\sigma}_x$, and $\bar{\tau}_{xz}^{EE}$ decrease, as shown in Figs. 8(a)-8(c). In Fig. 8(b), the axial stress displays more curvy nonlinear behavior transversely as the porosity volume fraction increases. Moreover, the maximum value is reached at $z = 0$ in the (0°) ply side. As ξ increases, the maximum transverse shear stress's location elevates a little, moving from $z = -0.28h$ to $z = -0.26h$ illustrated in Fig. 8(c).

Fig. 9(a) shows that the effect porosity model 3 has on the axial displacement is marginal. As the porosity volume fraction increases, both the axial stress and the transverse shear stress decrease as shown by Figs. 9(b) and 9(c). While as ξ increases $\bar{\sigma}_x$ decreases more at $z = 0$ compared to $z = -h/2$, the maximum axial stress is at the interface in the (0°) side. $\bar{\tau}_{\mathrm{xz}}^{EE}$ the highest value at $z = -0.29h$.

Fig. 10 compares porosity models effects at ξ = 0.2 on the cross-ply laminated beam's nondimensional stresses and displacements under the linear thermal load obtained by the present I-TBT theory. The beam's deflection, as depicted in Fig. 10(a), decreases as ξ increases for all models, with model 3 causing the least effect. For a constant ξ,

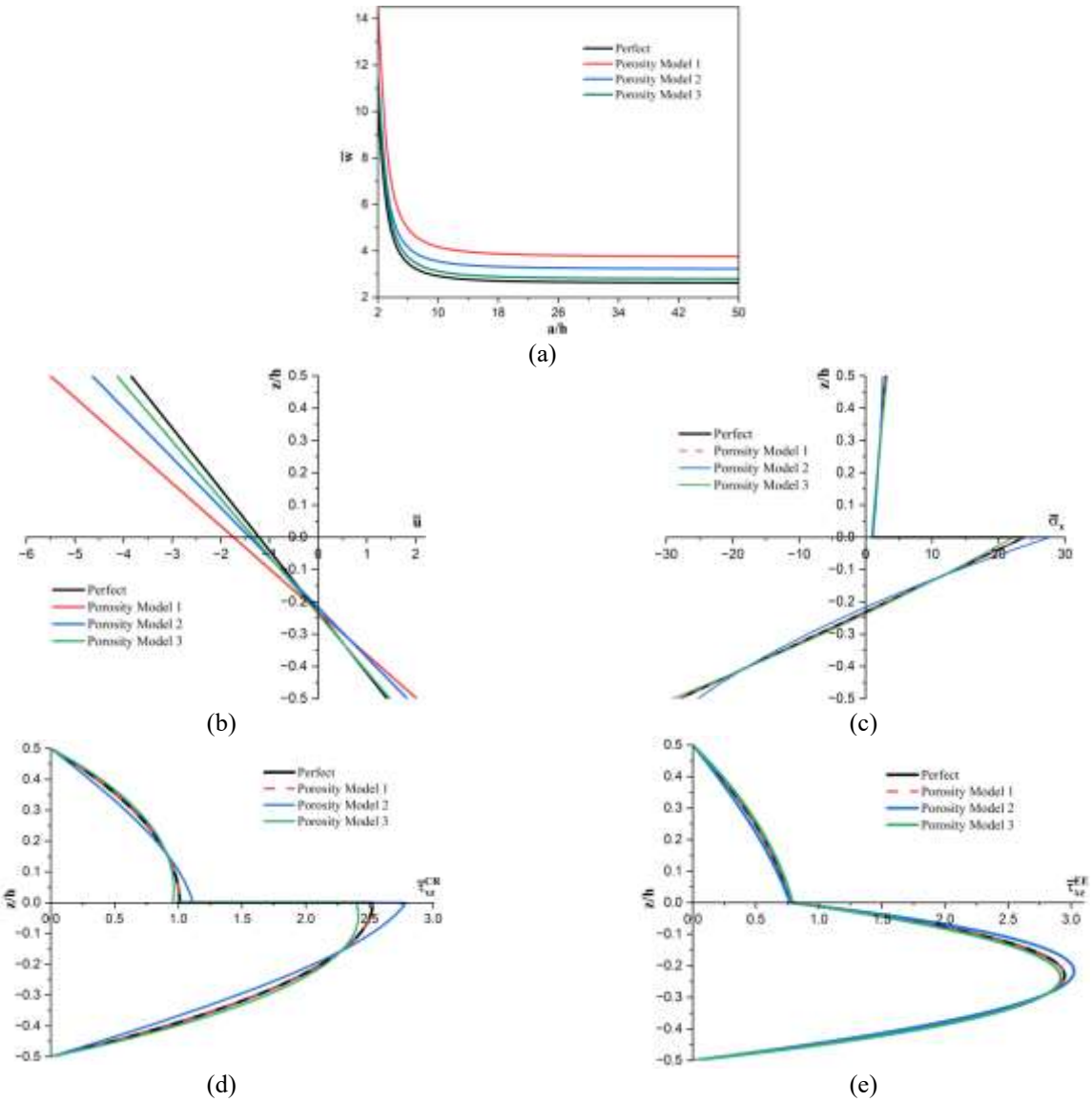

(a) (b) (c) (d) (e)

Fig. 6 Variation of dimensionless stresses and displacements for the (0°/90°) porous laminated beam under transverse sinusoidal mechanical load comparing all porosity models at ξ = 0.3 with $\frac{a}{h} = 4$: (a) lateral deflection $\bar{w}$ vs. *a/h*, (b) axial displacement $\bar{u}$ vs. *z/h*, (c) axial stress $\bar{\sigma}_x$ vs. *z/h*, (d) out-of-plane shear stress $\bar{\tau}_{xz}^{CR}$ vs. *z/h* and (e) out-of-plane shear stress $\bar{\tau}_{xz}^{EE}$ vs. *z/h*

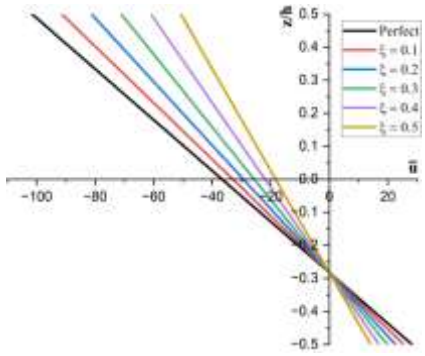

(a)

Fig. 7 Variation of dimensionless stresses and displacements for the (0°/90°) porous laminated beam under linearly varying sinusoidal thermal load according to porosity distribution model 1 with $\frac{a}{h} = 5$: (a) axial displacement $\bar{u}$ vs. *z/h*, (b) axial stress $\bar{\sigma}_x$ vs. *z/h* and (c) out-of-plane shear stress $\bar{\tau}_{xz}^{EE}$ vs. *z/h*

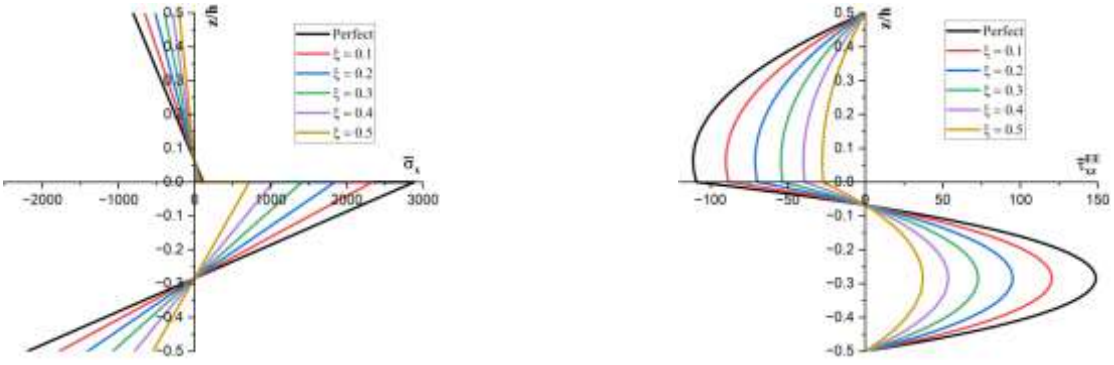

(b) (c)

Fig. 7 Continued-

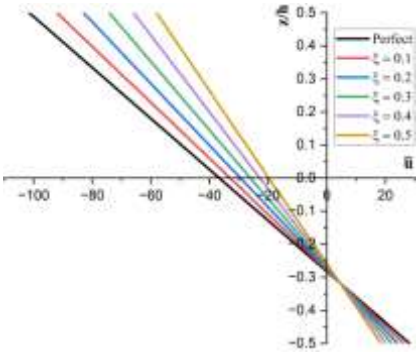

(a)

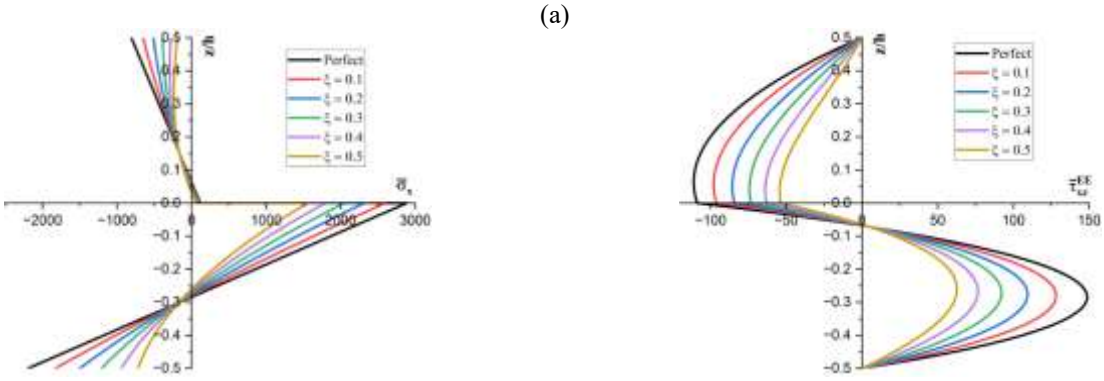

(b) (c)

Fig. 8 Variation of dimensionless stresses and displacements for the (0°/90°) porous laminated beam under linearly varying sinusoidal thermal load according to porosity distribution model 2 with $\frac{a}{h} = 5$: (a) axial displacement $\bar{u}$ vs. *z/h*, (b) axial stress $\bar{\sigma}_x$ vs. *z/h* and (c) out-of-plane shear stress $\bar{\tau}_{xz}^{EE}$ vs. *z/h*

Figs. 10(a)-10(d) indicate that the flexural response is affected the most by porosity model 1, followed by model 2. The axial displacement is insignificantly affected by porosity model 3.

5. Conclusions

This research uses an improved Timoshenko's beam theory (I-TBT) to conduct mechanical and thermal flexural analysis of simply supported porous cross-ply laminated beam. The present theory introduces a parabolic variation of the transverse shear stress and, therefore, doesn't require a shear correction factor. The governing equations were determined by the principle of virtual work, after which Navier's procedure was used to find the analytical solution for the simple support condition. In the mechanical load case, I-TBT's results were compared with those of Bernoulli Euler's CBT, Timoshenko's TBT, Sayyad-Ghugal's TrSDT, Reddy's HSDT, and exact elasticity theory as reported by Sayyad and Ghugal (2011). I-TBT provided the closest results to the elasticity theory compared with the other theories. The effects of porosity parameters variation were studied, and the following points were noticed:

- As the porosity volume fraction increases, $\bar{u}$ and $\bar{w}$ both increase the most using porosity distribution model 1, then 2.

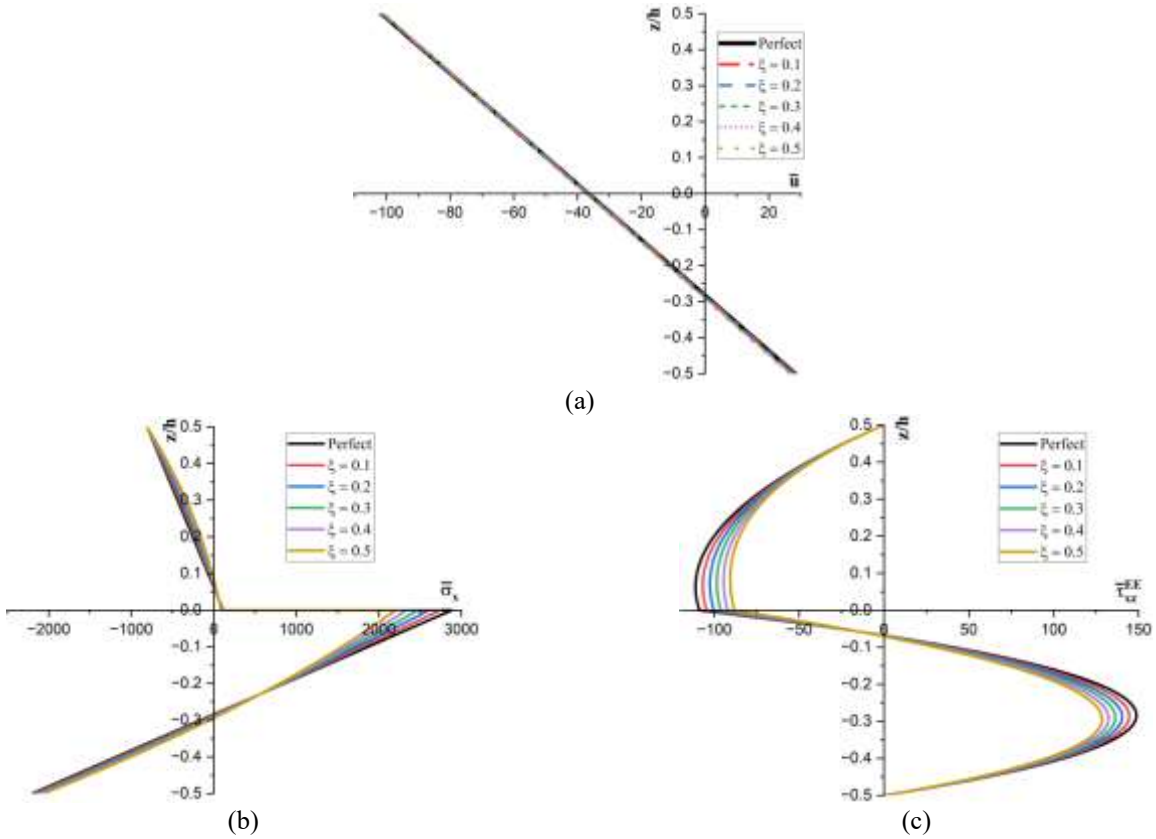

Fig. 9 Variation of dimensionless stresses and displacements for the (0°/90°) porous laminated beam under linearly varying sinusoidal thermal load according to porosity distribution model 3 with $\frac{a}{h} = 5$: (a) axial displacement $\bar{u}$ vs. *z/h*, (b) axial stress $\bar{\sigma}_x$ vs. *z/h* and (c) out-of-plane shear stress $\bar{\tau}_{xz}^{EE}$ vs. *z/h*

Table 3 Dimensionless displacements and stresses for (0°/90°) laminated perfect and porous beams with $\frac{a}{h} = 4$ under linearly varying along the thickness sinusoidal thermal load ($q = 0$)

Porosity Model and Volume Fraction		$\bar{u}\ (h/2)$	$\bar{w}$	$\bar{\sigma}_x\ (-h/2)$	$\bar{\tau}_{xz}^{EE}\ (0)$
CBT*	Perfect, $\xi = 0$	101.4844	41.2721	2188.1140	135.6737
TBT*		101.4938	41.2759	2188.1140	135.6736
I-TBT		101.494	41.276	2193.60	136.01
(I-TBT) Porosity Model 1	$\xi = 0.1$	91.345	37.148	1775.97	110.12
	$\xi = 0.2$	81.195	33.021	1402.64	86.97
	$\xi = 0.3$	71.046	28.893	1073.49	66.56
	$\xi = 0.4$	60.896	24.766	788.43	48.89
	$\xi = 0.5$	50.747	20.638	547.37	33.94
(I-TBT) Porosity Model 2	$\xi = 0.1$	92.068	37.621	1830.02	120.14
	$\xi = 0.2$	82.966	34.084	1501.42	105.31
	$\xi = 0.3$	74.231	30.681	1207.25	91.54
	$\xi = 0.4$	65.916	27.432	946.82	78.85
	$\xi = 0.5$	58.087	24.367	719.30	67.26
(I-TBT) Porosity Model 3	$\xi = 0.1$	101.244	41.080	2164.66	130.64
	$\xi = 0.2$	101.073	40.911	2136.47	125.37
	$\xi = 0.3$	100.989	40.773	2109.08	120.22
	$\xi = 0.4$	101.001	40.670	2082.54	115.18
	$\xi = 0.5$	101.120	40.604	2056.91	110.25

*From Ref. (Kulkarni and Ghugal 2018)

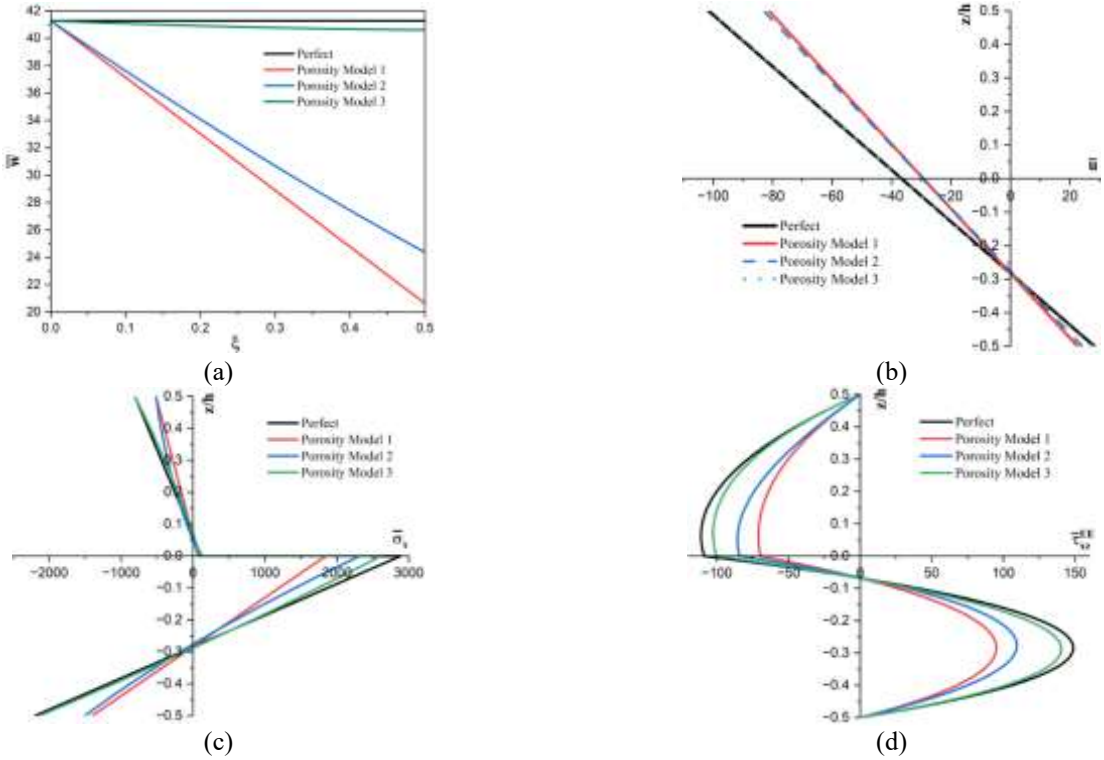

Fig. 10 Variation of dimensionless stresses and displacements for the (0°/90°) porous laminated beam under linearly varying sinusoidal thermal load comparing all porosity models with $\frac{a}{h} = 5$: (a) transverse deflection $\bar{w}$ vs. ξ, (b) axial displacement $\bar{u}$ vs. *z/h* at ξ = 0.2, (c) axial stress $\bar{\sigma}_x$ vs. *z/h* at ξ = 0.2 and (d) out-of-plane shear stress $\bar{\tau}_{xz}^{EE}$ vs. *z/h* at ξ = 0.2

- The highest influence on the normalized stresses is done by porosity model 2, followed by 3. While porosity model 1 doesn't seem to have an effect.
- As ξ increases for porosity model 2, the maximum magnitude for $\bar{\sigma}_x$ shifts from $z = -h/2$ to the plies interface in the (0°) lamina side. Whereas for model 3, it is always reached at $z = -h/2$.
- The maximum values of the transverse shear stresses $\bar{\tau}_{xz}^{CR}$ and $\bar{\tau}_{xz}^{EE}$ increase in porosity model 2 as ξ increases. In contrast, $\bar{\tau}_{xz}^{CR}$ and $\bar{\tau}_{xz}^{EE}$ maximum will decrease as ξ increases in model 3.
- Although the presence of porosity impacts stresses, the impact on the displacements seems much more pronounced.

The impact of the porosity characteristics was investigated for the linearly varying sinusoidal thermal load case, and the findings are summarized below.

- Most dimensionless stresses and displacements are affected by porosity model 1, then model 2.
- All the dimensionless stresses and displacements decrease as the porosity volume fraction increases.
- Porosity model 3 has negligible effects on the normalized displacements.
- For all porosity models and ξ values, the extreme magnitude of the axial stress is reached at $z = 0$ in the (0°) ply region.
- As ξ value increases from 0.1 to 0.5, the maximum transverse shear stress's position raises slightly, moving from $z = -0.28h$ to $z = -0.26h$, while for porosity models 1 and 3, the maximum is always at $\frac{z}{h} = -0.28$ and $\frac{z}{h} = -0.29$, respectively.

Acknowledgments

The authors would like to acknowledge the support provided by the Department of Civil & Environmental Engineering at King Fahd University of Petroleum & Minerals (KFUPM), Saudi Arabia. The support provided by the Interdisciplinary Research Center for Construction & Building Materials (IRC-CBM) at KFUPM, Saudi Arabia, is also greatly acknowledged.

References

Akavci, S.S. (2010), "Two new hyperbolic shear displacement models for orthotropic laminated composite plates", *Mech. Compos. Mater.*, **46**(2), 215-226. https://doi.org/10.1007/s11029-010-9140-3.

Arani, A.G., Pourjamshidian, M., Arefi, M. and Arani, M.R.G. (2019), "Thermal, electrical and mechanical buckling loads of sandwich nano-beams made of FG-CNTRC resting on Pasternak\'s foundation based on higher order shear deformation theory", *Struct. Eng. Mech.*, **69**(4), 439-455. https://doi.org/10.12989/sem.2019.69.4.439.

Aydogdu, M. (2009), "A new shear deformation theory for laminated composite plates", *Compos. Struct.*, **89**(1), 94-101. https://doi.org/10.1016/j.compstruct.2008.07.008.

Basem, A., Shadhar, M.H., Kadhim, Y.., Ranganathaswamy, M.K.,

Kumar, R., Abdullaeva, B., Mahariq, I., Althaqafi, E. and Islam, S. (2024), "Shear deformable-based kinematic model for static analysis of G-Ori composite panel", *Adv. Nano Res.*, **17**(6), 575-591. https://doi.org/10.12989/anr.2024.17.6.575.

Bhaskar, K., Varadan, T.K. and Ali, J.S.M. (1996), "Thermoelastic solutions for orthotropic and anisotropic composite laminates", *Compos. Part B: Eng.*, **27**(5), 415-420. https://doi.org/10.1016/1359-8368(96)00005-4.

Bina, R., Soltani Tehrani, M., Ahmadi, A., Ghanim Taki, A. and Akbarian, R. (2024), "Using 3D theory of elasticity for free vibration analysis of functionally graded laminated nanocomposite shells", *Steel Compos. Struct.*, **52**(4), 487-499. https://doi.org/10.12989/scs.2024.52.4.487.

Chen, D., Yang, J. and Kitipornchai, S. (2015), "Elastic buckling and static bending of shear deformable functionally graded porous beam", *Compos. Struct.*, **133**, 54-61. https://doi.org/10.1016/j.compstruct.2015.07.052.

Chen, W.R., Chiu, L.H. and Lin, C.H. (2024), "Vibration of elastically supported bidirectional functionally graded sandwich Timoshenko beams on an elastic foundation", *Struct. Eng. Mech*., **91**(2), 197-209. https://doi.org/10.12989/sem.2024.91.2.197.

Cui, Z., Yuan, Z. and Xi, C. (2024), "Engineering the future: Exploring the dynamic behavior of nanocomposite porous beams under the influence of nanoparticles", *Struct. Eng. Mech.*, **92**(6), 513-520. https://doi.org/10.12989/sem.2024.92.5.513.

Cui, Z., Yuan, Z. and Xi, C. (2024), "Engineering the future: Exploring the dynamic behavior of nanocomposite porous beams under the influence of nanoparticles", *Struct. Eng. Mech.*, **92**(6), 513-520. https://doi.org/10.12989/sem.2024.92.5.513.

Ebrahimi, F., hossein, M., fallahi, G. and Ziazi, A. (2024), "Porosity effects on the buckling and post buckling of metamaterial sandwich toroidal shell segments", *Steel Compos. Struct*., **53**(3), 313-326. https://doi.org/10.12989/scs.2024.53.3.313.

Ekmon, M.N., Roland, N.N.A., Renaud, N.G.J., Joseph, N.A. and Robert, N. (2024), "New laminate constitutive equations for analysing the mechanical behavior of anisotropic plates and shells", *Comput. Concrete*, **34**(5), 591-609. https://doi.org/10.12989/cac.2024.34.5.591.

Emam, S.A. (2011), "Analysis of shear-deformable composite beams in postbuckling", *Compos. Struct.*, **94**(1), 24-30. https://doi.org/10.1016/j.compstruct.2011.07.024.

Fang, W., Yu, T., Van Lich, L. and Bui, T.Q. (2019), "Analysis of thick porous beams by a quasi-3d theory and isogeometric analysis", *Compos. Struct.*, **221**, 110890. https://doi.org/10.1016/j.compstruct.2019.04.062.

Foroutan, K. and Dai, L. (2024), "Nonlinear free and forced vibrations of oblique stiffened porous FG shallow shells embedded in a nonlinear elastic foundation", *Struct. Eng. Mech.*, **89**(1), 33-46. https://doi.org/10.12989/sem.2024.89.1.033.

Frih, A., Bourada, F., Kaci, A., Bouremana, M., Tounsi, A., Al-Osta, M.A., Khedher, K.M. and Salem, M.A. (2023), "A novel hyperbolic integral-Quasi-3D theory for flexural response of laminated composite plates", *Geomech. Eng.*, **34**(3), 233-250. DOI: https://doi.org/10.12989/gae.2023.34.3.233.

Ghalami-Choobar, M., Liaghat, G., Sadighi, M., Ahmadi, H., Razmkhah, O. and Aboutorabi, A. (2018), "Static analysis of highly anisotropic laminated beam using unified zig-zag theory subjected to mechanical and thermal loading", *Int. J. Mech. Sci.*, **141**, 491-501. https://doi.org/10.1016/j.ijmecsci.2018.04.030.

Grover, N., Maiti, D.K. and Singh, B.N. (2013), "A new inverse hyperbolic shear deformation theory for static and buckling analysis of laminated composite and Sandwich Plates", *Compos. Struct.*, **95**, 667-675. https://doi.org/10.1016/j.compstruct.2012.08.012.

Hadji, L., Madan, R., Atmane, H.A., Bernard, F., Zouatnia, N. and Safa, A. (2024), "Thermal buckling Analysis of functionally graded plates using trigonometric shear deformation theory for temperature-dependent material properties", *Struct. Eng. Mech.*, **91**(6), 539-549. https://doi.org/10.12989/sem.2024.91.6.539.

He, Y.J. and She, G.L. (2024), "Nonlinear forced vibration of imperfect FG beams with hygro-thermal factor", *Struct. Eng. Mech.*, **92**(2), 163-172. https://doi.org/10.12989/sem.2024.92.2.163.

He, Y.J. and She, G.L. (2024), "Nonlinear forced vibration of imperfect FG beams with hygro-thermal factor", *Struct. Eng. Mech.*, **92**(2), 163-172. https://doi.org/10.12989/sem.2024.92.2.163.

Kapuria, S., Dumir, P.C. and Ahmed, A. (2003), "An efficient higher order zigzag theory for composite and sandwich beams subjected to thermal loading", *Int. J. Solids Struct.*, **40**(24), 6613-6631. https://doi.org/10.1016/j.ijsolstr.2003.08.014.

Karama, M., Afaq, K.S. and Mistou, S. (2003), "Mechanical behaviour of laminated composite beam by the new multi-layered laminated composite structures model with transverse shear stress continuity", *Int. J. Solids Struct.*, **40**(6), 1525-1546. https://doi.org/10.1016/s0020-7683(02)00647-9.

Khdeir, A.A. and Reddy, J.N. (1997), "An exact solution for the bending of thin and thick cross-ply laminated beams", *Compos. Struct.*, **37**(2), 195-203. https://doi.org/10.1016/s0263-8223(97)80012-8.

Kulkarni, S.K. and Ghugal, Y.M. (2018), "Flexural analysis of composite laminated beams subjected to thermo-mechanical loads", *J. Serbian Soc. Comput. Mech.*, **12**(1), 52-79. https://doi.org/10.24874/jsscm.2018.12.01.05.

Kumar, R. and Kumar, A. (2022), "Flexural analysis of laminated composite porous plate", *Asian J. Civil Eng.*, **24**(3), 673-692. https://doi.org/10.1007/s42107-022-00523-y.

Kumar, R., Kumar, A. and Panda, S.K. (2015), "Parametric resonance of composite skew plate under non-uniform in-plane loading", *Struct. Eng. Mech.*, **55**(2), 435-459. https://doi.org/10.12989/sem.2015.55.2.435.

Li, Y.P. and She, G.L. (2024), "Nonlinear resonance of magneto-electro-thermal-elastic plates with geometric imperfection", *Comput. Concrete*, **34**(3), 267-277. https://doi.org/10.12989/cac.2024.34.3.267.

Liu, Z., Zhu, K., Wen, X. and Kumar, A. (2024), "Nonlinear vibration analysis of FG porous shear deformable cylindrical shells covered by CNTs-reinforced nanocomposite layers considering neutral surface exact position", *Adv. Nano Res.*, **17**(1), 61-73. https://doi.org/10.12989/anr.2024.17.1.061.

Madenci, E. and Özütok, A. (2021), "Variational approximate for high order bending analysis of laminated composite plates", *Struct. Eng. Mech.*, **73**(1), 97-108. https://doi.org/10.12989/sem.2020.73.1.097.

Mantari, J.L. and Canales, F.G. (2016), "A unified quasi-3d HSDT for the bending analysis of laminated beams", *Aerosp. Sci. Technol.*, **54**, 267-275. https://doi.org/10.1016/j.ast.2016.04.026.

Matsunaga, H. (2000), "Vibration and stability of cross-ply laminated composite plates according to a global higher-order plate theory", *Compos. Struct.*, **48**(4), 231-244. https://doi.org/10.1016/s0263-8223(99)00110-5.

Mehar, K. and Panda, S.K. (2018), "Nonlinear finite element solutions of thermoelastic flexural strength and stress values of temperature dependent graded CNT-reinforced sandwich shallow shell structure", *Struct. Eng. Mech.*, **67**(6), 565-578. https://doi.org/10.12989/sem.2018.67.6.565.

Murugesan, N. and Rajamohan, V. (2015), "Investigation on interlaminar shear stresses in laminated composite beam under thermal and mechanical loading", *Steel Compos. Struct.*, **18**(3),

583-601. https://doi.org/10.12989/scs.2015.18.3.583.

Osman, T., Mohamed, S.A., Eltaher, M.A., Alazwari, M.A. and Mohamed, N. (2024), "Vibration of bio-inspired laminated composite beams under varying axial loads", *Steel Compos. Struct.*, **50**(1), 25-43. https://doi.org/10.12989/scs.2024.50.1.025.

Ozbey, M.B., Cuma, Y.C., Deneme, I.O. and Calim, F. F. (2024), "Free and forced vibration analysis of FG-CNTRC viscoelastic plate using high shear deformation theory", *Adv. Nano Res.*, **16**(4), 413-426. https://doi.org/10.12989/anr.2024.16.4.413.

Pham, Q.H., Nguyen, P.C. and Tran, V.K. (2024), "Effects of hygro-thermal environment on dynamic responses of variable thickness functionally graded porous microplates", *Steel Compos. Struct.*, **50**(5), 563-581. https://doi.org/10.12989/scs.2024.50.5.563.

Pham, Q.H., Nguyen, P.C. and Tran, V.-K. (2024), "Effects of hygro-thermal environment on dynamic responses of variable thickness functionally graded porous microplates", *Steel Compos. Struct.*, **50**(5), 563-581. https://doi.org/10.12989/scs.2024.50.5.563.

Plevris, V., Hadji, L. and Madan, R. (2024). "Exploring porosity impact on the free vibration of FG plates using trigonometric shear deformation theory", *Struct. Eng. Mech.*, **92**(3), 267-275. https://doi.org/10.12989/sem.2024.92.3.267.

Rajendran, S., Loganathan, R., Yaylaci, M., Yaylaci, E.U. and Ozdemir, M.E. (2024), "Vibration of piezo-magneto-thermoelastic FG nanobeam submerged in fluid with variable nonlocal parameter", *Adv. Nano Res.*, **16**(5), 489-500. https://doi.org/10.12989/anr.2024.16.5.489.

Reddy, J.N. (2004), *Mechanics of laminated composite plates and shells: Theory and analysis*. CRC Press.

Sahoo, R. and Singh, B.N. (2013), "A new inverse hyperbolic zigzag theory for the static analysis of laminated composite and sandwich plates", *Compos. Struct.*, **105**, 385-397. https://doi.org/10.1016/j.compstruct.2013.05.043.

Sayyad, A.S. and Ghugal, Y.M. (2011), "Effect of transverse shear and transverse normal strain on bending analysis of cross-ply laminated beams", *Int. J. Appl. Math. Mech.*, **7**(12), 85-118.

She, G.L., Li, Y.P., He, Y. and Song, J.P. (2024), "Thermal post-buckling analysis of graphene platelets reinforced metal foams beams with initial geometric imperfection", *Comput. Concrete*, **33**(3), 241-250. https://doi.org/10.12989/cac.2024.33.3.241.

Shen, X., Li, T., Xu, L., Kiarasi, F., Babaei, M. and Asemi, K. (2024), "Free vibration analysis of FG porous spherical cap reinforced by graphene platelet resting on Winkler foundation", *Adv. Nano Res.*, **16**(1), 11-26. https://doi.org/10.12989/anr.2024.16.1.011.

Soldatos, K.P. (1992), "A transverse shear deformation theory for homogeneous monoclinic plates", *Acta Mechanica*, **94**(3-4), 195-220. https://doi.org/10.1007/bf01176650.

Srinivasan, R., Dattaguru, B. and Singh, G. (2019), "Exact solutions for laminated composite beams using a unified state space formulation", *Int. J. Comput. Method. Eng. Sci. Mech.*, **20**(4), 319-334. https://doi.org/10.1080/15502287.2019.1644394.

Tanigawa, Y., Murakami, H. and Ootao, Y. (1989), "Transient thermal stress analysis of a laminated composite beam", *J. Therm. Stresses*, **12**(1), 25-39. https://doi.org/10.1080/01495738908961952.

Touratier, M. (1991), "An efficient standard plate theory", *Int. J. Eng. Sci.*, **29**(8), 901-916. https://doi.org/10.1016/0020-7225(91)90165-y.

Turan, F. (2024), Free vibration response of multi-layered plates with trigonometrically distributed porosity based on the higher-order shear deformation theory", *Steel Compos. Struct.*, **53**(1), 77-90. https://doi.org/10.12989/scs.2024.53.1.077.

Vidal, P. and Polit, O. (2006), "A thermomechanical finite element for the analysis of rectangular laminated beams", *Finite Elem. Anal. Des.*, **42**(10), 868-883. https://doi.org/10.1016/j.finel.2006.01.005.

Vidal, P. and Polit, O. (2009), "A refined sine-based finite element with transverse normal deformation for the analysis of laminated beams under thermomechanical loads", *J. Mech. Mater. Struct.*, **4**(6), 1127-1155. https://doi.org/10.2140/jomms.2009.4.1127.

Vinyas, M., Harursampath, D. and Kattimani, S.C. (2020), "Thermal response analysis of multi-layered magneto-electro-thermo-elastic plates using higher order shear deformation theory", *Struct. Eng. Mech.*, **73**(6), 667-684. https://doi.org/10.12989/sem.2020.73.6.667.

Xu, J. and She, G.L. (2023), "The effects of temperature and porosity on resonance behavior of graphene platelet reinforced metal foams doubly-curved shells with geometric imperfection", *Geomech. Eng.*, **35**(1), 81-93. https://doi.org/10.12989/gae.2023.35.1.081.

Yüksel, Y.Z. and Akbaş, S.D. (2019), "Buckling analysis of a fiber reinforced laminated composite pPlate with porosity", *J. Comput. Appl. Mech*., **50**(2), 375-380. https://doi.org/10.22059/jcamech.2019.291967.448.

Zhang, Y.W., She, G.L., Gan, L.L. and Li, Y.P. (2023), "Thermal post-buckling behavior of GPLRMF cylindrical shells with initial geometrical imperfection", *Geomech. Eng.*, **32**(6), 615-625. https://doi.org/10.12989/gae.2023.32.6.615.

CC